

Sodium Compatibility of Recently-Developed Optimized Grade 92 Steel for Advanced Fast Reactors

Meimei Li¹, Krishnamurti Natesan¹, Weiyang Chen¹, Yoichi Momozaki¹

¹Argonne National Laboratory (ANL), Argonne, IL, U.S.A

E-mail contact of main author: mli@anl.gov

Abstract.

This paper presents the results of sodium compatibility of optimized Grade 92 steel recently developed in the United States for applications in advanced sodium-cooled fast reactors. Optimized Grade 92 (Fe-9Cr-0.5Mo-2W-V,Nb) is a variant of commercially available Grade 92 ferritic-martensitic steels with tighter control of chemistry to achieve improved high temperature performance. Several heats of optimized Grade 92 with or without thermo-mechanical treatment were investigated in liquid sodium environments to evaluate their long-term performance.

Sodium exposure experiments were conducted at 550, 600 and 650°C in forced convection sodium loops at the Argonne National Laboratory (ANL). The oxygen content of sodium was controlled by the cold-trapping method to achieve ~1 wppm oxygen level. Post sodium-exposure examinations included weight and thickness measurements, cross-sectional examinations, micro-hardness measurements, microstructural characterization, and tensile tests at the sodium exposure temperature. Data of sodium-exposed specimens were compared with thermal aging data of the same heat of optimized Grade 92 to separate the effects of sodium exposures and thermal aging. Optimized Grade 92 showed an insignificant weight loss after exposures to sodium at 550-650°C. Sodium exposures at 650°C have a much stronger effect on the tensile strength than thermal exposures at 650°C, but not at 600 and 550°C with available data. Microstructural characterization of optimized Grade 92 after sodium exposure at 650°C showed drastic microstructural changes manifested by reduction in dislocation density, subgrain coarsening, $M_{23}C_6$ and MX coarsening and dissolution, and precipitation of Laves phase.

Key Words: Sodium compatibility, microstructure, tensile property, High-Cr ferritic-martensitic steels.

1. Introduction

Optimized Grade 92 (Fe-9Cr-0.5Mo-2W-V,Nb) is a variant of commercially available Grade 92 ferritic-martensitic steels with tighter control of chemistry and thermo-mechanical treatment to achieve improved high temperature performance. Optimized G92 with and without thermomechanical treatment (TMT) has been developed in the United States for its potential applications for structural components in advanced sodium-cooled fast reactors. Though the alloy shows enhanced creep properties, good cross-weld creep performance, and comparable fatigue/creep-fatigue performance to commercial G92 steels [1], its sodium compatibility and the effect of sodium exposures on microstructure and mechanical properties have not been fully addressed.

Structural alloys can undergo a variety of interactions upon exposure to liquid sodium. The extent of the interaction depends upon the exposure condition of temperature, temperature gradient, sodium velocity and purity, the materials of construction, and external sources and sinks for the constituent elements of the structural materials. The interactions can be broadly classified into either metallic or nonmetallic element mass transfer. Metallic element transfer can cause dissolution of metallic elements into sodium, or by formation of corrosion products on the metallic surfaces that subsequently erode/spall into the flowing sodium. Nonmetallic

elements such as carbon and nitrogen are known to migrate in structural materials/sodium systems as a result of chemical activity differences that occur in isothermal or non-isothermal systems. Ferritic steels are susceptible to decarburization when exposed to high temperature sodium because of their inherently higher carbon activity and large carbon diffusion coefficient [2-5]. High-Cr ferritic-martensitic steels, e.g. Fe-9Cr-Mo steels are more resistant to carbon transfer than Fe-2.25Cr-Mo steel in sodium environments [2-5], and are of great interest for structural applications in advanced sodium-cooled fast reactors. This paper reports the experimental data of sodium exposure tests of optimized G92 conducted at 550-650°C and detailed investigations of the effect of sodium exposures on corrosion behavior, microstructure, and tensile properties of optimized G92.

2. Experimental Procedure

2.1. Materials and Specimens

The chemistry of optimized G92 (Fe-9Cr-0.5Mo-2W-V,Nb) steel is within ASTM A213/335 chemistry specifications but with tighter control. Its mechanical property does not meet the specifications. Several heats of optimized G92, i.e., Opt. G92-3, Opt. G92-4, Opt. G92-4T, and Opt. G92-8T were examined together with a commercial grade of G92 steel. Commercial G92 and heats of Opt. G92-3 and Opt. G92-4 of optimized G92 were in the normalized and tempered condition, and heats of Opt. G92-4T, and Opt. G92-8T of optimized G92 received an additional thermo-mechanical treatment (TMT), and “T” denotes the TMT condition. All materials were provided by the Oak Ridge National Laboratory (ORNL).

Subsize sheet-type tensile specimens with extended grips were used in sodium exposure tests and subsequent microstructural characterization and tensile testing. The tensile specimen has nominal gage dimensions of $7.62 \times 1.52 \times 0.76$ mm. The extended grip sections were used for microstructural characterization to ensure that the microstructure and tensile property data were obtained on the same sodium-exposed specimen. Tensile specimens were electrical-discharge-machined with the gage parallel to the rolling direction.

2.2. Forced Convection Sodium Loops and Sodium Exposure Tests

Two forced convection sodium loops were constructed at the Argonne National Laboratory (ANL) for sodium exposure tests of advanced materials. The Sodium Materials Test Loop 1 (SMT-1) (shown in Fig. 1(a)) consists of a single specimen-exposure vessel with an electromagnetic pump, two electromagnetic flow meters, an economizer, and a cold trap, with the total amount of sodium in the loop of approximately 10 kg. The vessel has three penetrations at the top for sample loading as well as small penetrations for a level probe, thermocouple, and argon/vacuum line. The maximum operating pressure and temperature of the specimen vessel are 5 psig and 700°C. The Sodium Materials Test Loop 2 (SMT-2) (shown in Fig. 1(b)) is a dual sample-vessel loop for sodium exposure tests at two temperatures. The maximum operating pressure and temperature for the two sample vessels are 5 psig and 750°C, and the total amount of sodium in the loop is approximately 20 kg. Each vessel has two penetrations at the top for loading samples as well as smaller penetrations for a level probe, thermocouple, and argon/vacuum line. Both loops are constructed of austenitic stainless steels. The oxygen content of the sodium is controlled by the cold trap in both loops. The temperature of the cold trap is maintained at 125°C to ensure that the oxygen concentration is at ~1 wppm during specimen exposure.

Sodium exposure tests were performed at 550°C for up to 11,233 h for optimized G92 and 13,941 h for commercial G92, at 600°C for up to 16,233 h for optimized G92 and 15,562 h for commercial G92, and at 650°C for up to 9,735 h for optimized G92 and 19,952 h for commercial G92. After each exposure test, the specimen was removed from the loop for post-sodium-exposure examination. Specimens were cleaned with alcohol with final cleaning with water to remove any sodium residues.

Thermal aging tests were conducted at 550 - 650°C in vacuum on the same materials for comparable exposure times to separate the effects of thermal aging and sodium exposures.

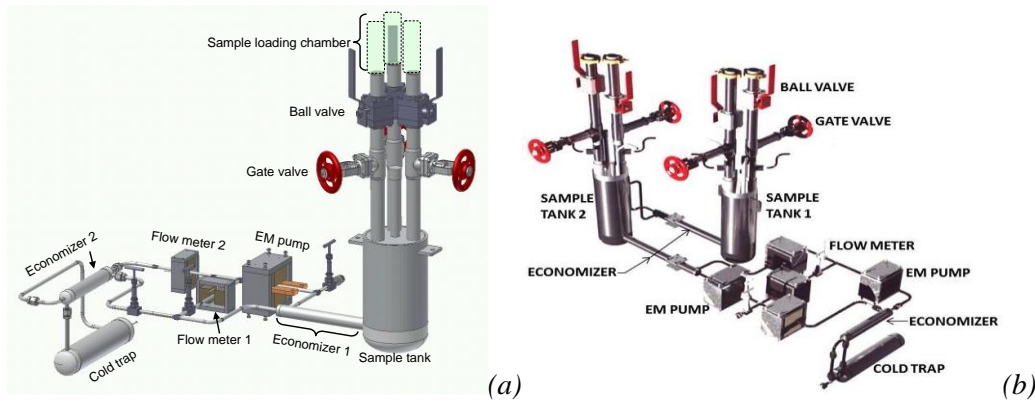


Figure 1. Isometric view of (a) Sodium Materials Test Loop 1 (SMT-1) and (b) Sodium Materials Test Loop 2 (SMT-2) at ANL.

2.3. Post-Sodium Exposure Examinations

After being removed from the sodium loop and cleaned, specimens were visually inspected and recorded by a digital camera. Mass and thickness measurements were conducted before and after each sodium exposure test to determine the mass and thickness changes. Each specimen was weighed three times using an OHAUS Model AP250 analytical balance to a precision of 10 μg . The thickness of each specimen was measured three times using a micrometer to a precision of 3 μm . The post-sodium-exposure weight and thickness measurements were compared with the initial weight and thickness data obtained prior to Na exposures. If only non-destructive (weight and thickness) measurements were performed on a specimen, the specimen was reloaded into the sodium loop for continued exposure.

Destructive examinations after a sodium exposure test included microstructural characterization, micro-hardness measurements, and tensile tests. The extended grip sections of the exposed tensile specimen were cut from both ends for microstructural analysis and micro-hardness measurements. Metallographic specimens were made from the cross section for examination of microstructure by optical microscopy (OM) and scanning electron microscopy (SEM), and micro-hardness measurements. The metallographic specimen was chemically etched with an etchant of 5 ml HNO_3 , 1 ml HF , and 50 ml H_2O . Thin foil specimens of 3-mm in diameter were made from the specimen grips for microstructural characterization by transmission electron microscopy (TEM). Specimens were electropolished to perforation using a Tenupol twin-jet polishing unit. Carbon extraction replicas were also made for precipitate characterization by TEM.

Tensile specimens were tested under uniaxial tension to examine the effects of thermal and sodium exposures on tensile properties. Tensile tests were performed in an electromechanical testing system equipped with a three-zone air furnace. The applied load

was recorded by a load cell; the specimen displacement was measured by the crosshead extension. The engineering tensile properties were determined from analysis of load versus displacement data files. Thermally-aged or sodium-exposed specimens were tested at the thermal or sodium exposure temperature at a nominal strain rate, 0.001 s^{-1} .

3. Results

3.1. Corrosion behavior

After sodium exposures, specimens lost surface finish, but the surface remained smooth, and no spallation or surface deterioration was visually observable. Weight changes due to sodium exposures are shown in Figs. 2(a) and (b) for 600 and 650°C, respectively, for various heats of optimized G92 and a commercial G92. The data represent an average of three measurements of one specimen before and after a sodium exposure. Both optimized and commercial G92 showed weight losses after sodium exposures at 650°C, while the weight changes after sodium exposures at 600°C scatter around zero with a few outliers ($>0.05\%$). The weight losses of optimized and commercial G92 at 650°C showed a continuous increase with the exposure time and reached a plateau at $\sim 10,000 \text{ h}$. The weight loss was no more than 0.1% after sodium exposure up to $\sim 20,000 \text{ h}$, corresponding to a corrosion rate $<1 \mu\text{m/y}$. All heats of optimized G92 showed similar behavior. SEM images of cross-section specimens show little changes across the specimen thickness. This is expected behavior since the oxygen concentration is the primary cause for corrosion of a material, and it was controlled to $\sim 1 \text{ wppm}$ in the sodium experiments, which results in acceptable corrosion of high-Cr ferritic steels [2,3].

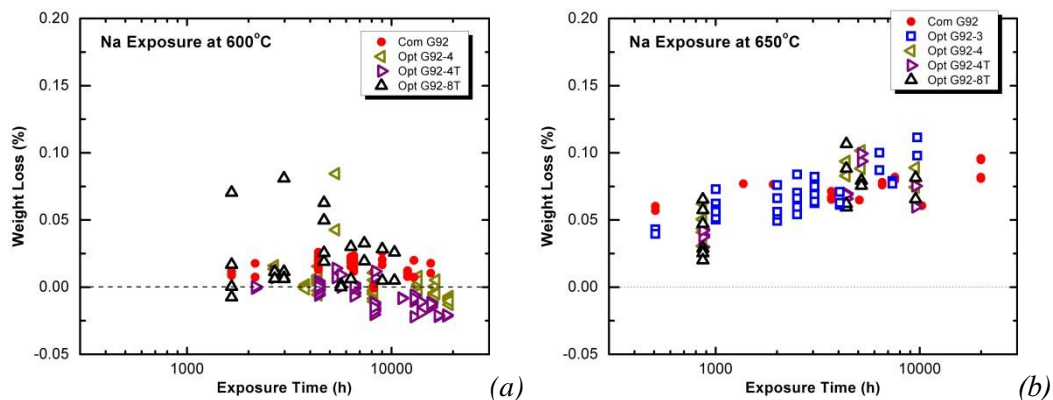


Figure 2. Weight changes for different heats of optimized G92 (Opt. G92) and commercial G92 (Com. G92) after sodium exposures at (a) 600°C and (b) 650°C.

3.2. Effect of Sodium Exposures on Tensile Property

Figure 3 compares the effects of sodium and thermal exposures on tensile property of optimized G92 and commercial G92 tested at 550-650°C. The ultimate tensile strength (UTS) as a function of exposure time is given in Figs. 5(a), (c), and (e), and the total elongation as a function of exposure time is given in Figs. 5(b), (d), and (f), for the exposure temperatures of 550, 600, and 650°C, respectively. The results indicate that sodium exposures at 550 and 600°C caused virtually no additional effect on the UTS and total elongation when compared with thermally-aged specimens of optimized and commercial G92 up to $\sim 16,000 \text{ h}$, while sodium exposures at 650°C have a much stronger effect on the UTS of all heats of optimized G92 and commercial G92 than thermal exposures alone under comparable temperature and

time conditions. The total elongation of optimized and commercial G92 remained >15% after both thermal and sodium exposures at 650°C.

The reductions in tensile strength from sodium exposures at 650°C varied among different heats of optimized G92. Heats of Opt. G92-3 and Opt. G92-8T have the highest UTS in the as-received condition. The UTS of these two heats was reduced by ~50% after sodium exposure and ~30% after thermal exposure at 650°C for 5,000 h. Heats of Opt. G92-4 and Opt. G92-4T have the lowest UTS prior to Na exposures, and their UTS values were reduced by ~40% after sodium exposure and ~10% after thermal exposure at 650°C for 5,000 h. While the commercial G92 has moderate UTS compared to various heats of optimized G92, its UTS was decreased by 37% from sodium exposures at 650°C, 15% from thermal exposures at the same temperature. The total elongation of all thermally-aged and sodium exposed specimens of optimized and commercial G92 remained >10%.

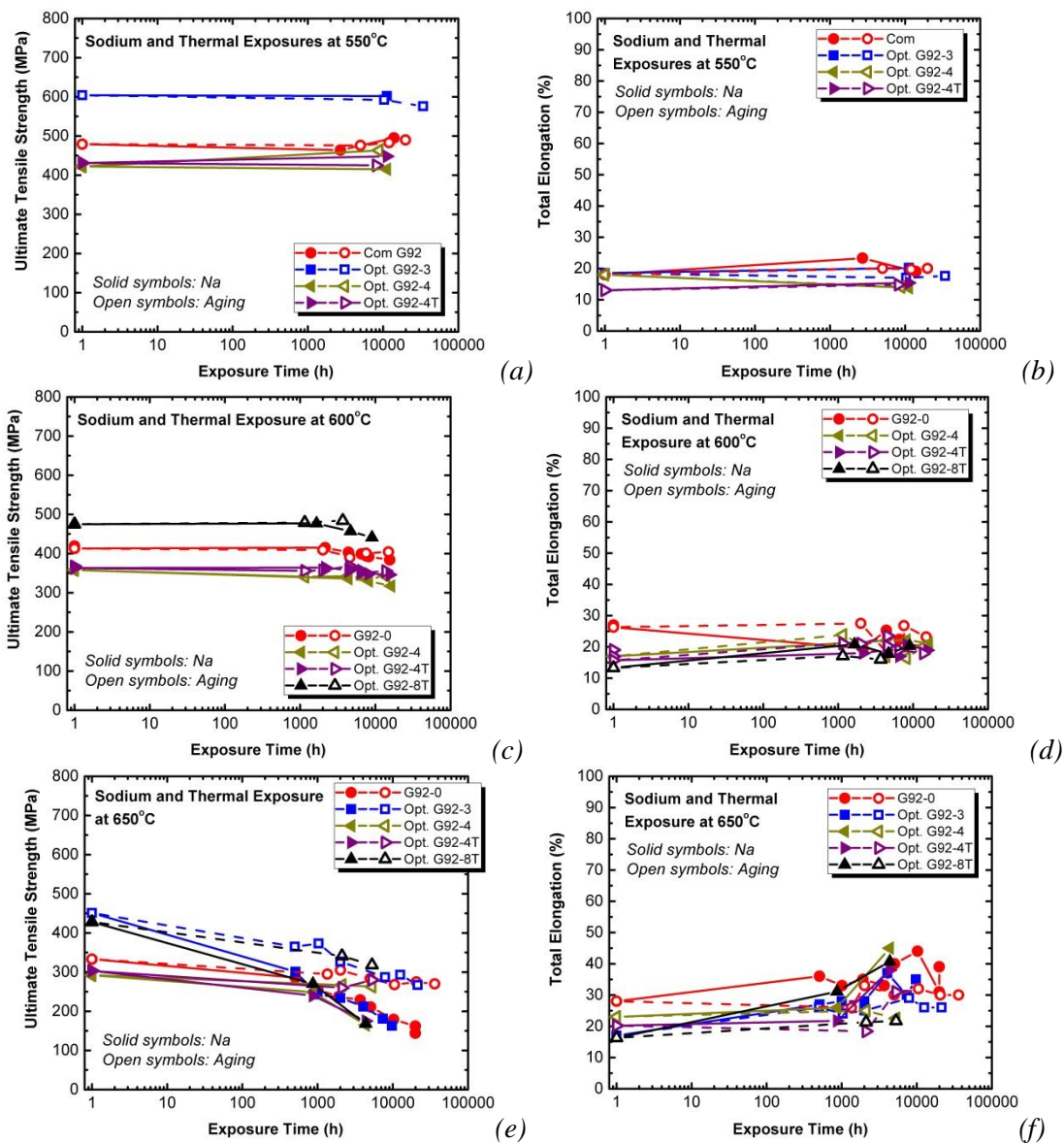


Figure 3. (a), (c), (e) Ultimate tensile strength and (b), (d), (f) total elongation as a function of exposure time after thermal or sodium exposures at 550, 600 and 650 °C for optimized G92 and commercial G92. Tensile tests were conducted at the exposure temperature.

3.3. Effect of Sodium Exposures on Microstructure

Microstructural characterization was conducted on heat of Opt. G92-4 of optimized G92 in the as-received condition, after thermal aging for 5,284 h at 650°C, and after sodium exposure for 4,370 h at 650°C. The microstructure of the as-received Opt. G92-4 has tempered martensitic structure with a high density of dislocations, $M_{23}C_6$ carbides decorated primarily along grain or subgrain boundaries, and a fine distribution of vanadium/niobium carbonitrides (MX) within subgrains. Both thermal and sodium exposures at 650°C caused significant microstructural changes, e.g. dislocation density and structural changes, subgrain coarsening, carbides and carbonitrides coarsening or dissolution, and precipitation of a new phase, intermetallic Laves phase. Figures 4 (a) – (d) show representative TEM/SEM images of subgrains, dislocations within a subgrain, $M_{23}C_6$, MX and Laves phase precipitates in the specimen exposed to sodium for 4,370 h at 650°C. Quantitative measurements of dislocation densities within subgrains, subgrain widths, and size distributions of $M_{23}C_6$, MX and Laves phase precipitates were made on the three Opt. G92-4 specimens, and the data are compared in Fig. 4(e). Note that the sodium exposure time was 914 h shorter than the thermal exposure.

Microstructural changes in Opt. G92-4 during sodium exposure were much more pronounced than during thermal exposure at 650°C. Subgrains coarsened rapidly during the sodium exposure. The mean width of subgrains in the sodium-exposed Opt. G92-4 was 899 nm, while the mean width of subgrains in the thermally-aged Opt. G92-4 was 492 nm. The dislocation density in the sodium-exposed Opt. G92-4 specimen was reduced significantly, with the density of $2.0 \times 10^{13}/m^2$, compared to $9.4 \times 10^{13}/m^2$ in the as-received Opt. G92-4 and $9.3 \times 10^{13}/m^2$ in the thermally-aged Opt. G92-4.

Coarsening of $M_{23}C_6$ carbides was observed in both thermally-aged and sodium-exposed Opt. G92-4 specimens. The mean size of $M_{23}C_6$ precipitates in the sodium-exposed Opt. G92-4 specimen was 176 nm, larger than that in the thermally-aged Opt. G92-4 specimen, 119 nm. A much lower number density of $M_{23}C_6$ carbides was observed in the sodium-exposed specimen than in the as-received and thermally-aged specimens. The larger mean size of $M_{23}C_6$ carbides measured in the sodium-exposed specimen may be attributed to the dissolution of smaller sizes of $M_{23}C_6$ particles in the sodium environment, which influenced the size distribution of $M_{23}C_6$ particles.

TEM examination of the sodium-exposed specimen showed a very low density of MX precipitates, precluding a reliable measurement of MX particles, and no data of MX precipitates was reported in Fig. 4(e) for the sodium-exposed specimen. Thermal exposure at 650°C caused coarsening of MX particles in Opt. G92-4.

Precipitation of Laves phase occurred during thermal and sodium exposures at 650°C in Opt. G92-4. Laves phase precipitates were distributed primarily along grain/subgrain boundaries. They coarsened more rapidly in the sodium environment than under thermal exposure.

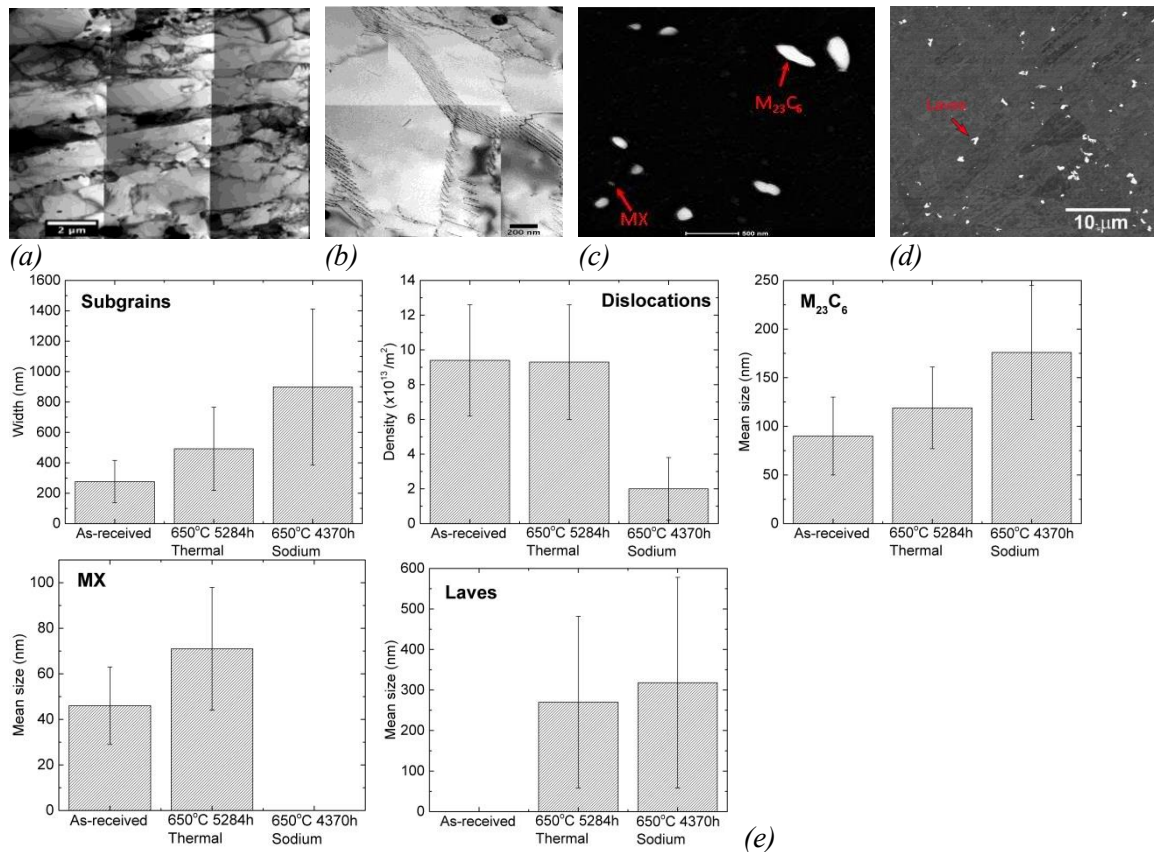


Figure 4. Microstructure of optimized G92-4 after sodium exposure for 4,370 h at 650 °C (a) TEM image of subgrains, (b) TEM image of dislocations, (c) TEM image of $M_{23}C_6$ and MX precipitates, (d) SEM image of Laves phase, and (e) comparison of subgrain width, dislocation density, mean sizes of $M_{23}C_6$, MX and Laves phase particles in the as-received, thermally-aged (650 °C/5,284h), and sodium-exposed (650 °C/4,370h) specimens.

4. Discussion

The high temperature strength and creep resistance of ferritic-martensitic steels, e.g. Grade 91 and Grade 92 steels rely on solid solution hardening of Mo and/or W, dislocation hardening, boundary and sub-boundary hardening, and precipitation hardening [7]. Prior to sodium exposures, the strength of optimized G92 relies on tempered martensitic microstructure stabilized by $M_{23}C_6$ carbides, a fine distribution of vanadium/niobium carbonitrides MX ((V,Nb)(C,N)), and solution strengthening by Mo and W. Maintenance of the precise microstructure during service in reactors is key to retain its superior performance. Our experimental data have shown that exposure of optimized G92 to high-temperature sodium can result in significant microstructural changes, leading to degradation of high temperature tensile strength. The effect of sodium exposures was most pronounced at 650 °C, and insignificant at 550-600 °C for the exposure times investigated.

It is important to note that the alloy undergoes microstructural changes due to both thermal exposures and sodium exposures at high temperature. The more pronounced microstructural changes observed in the specimen exposed to sodium than in the specimen thermally aged at 650 °C (Fig. 4) may be understood by combined effects of thermal aging and interstitial element transfer in liquid sodium. Non-metallic elements such as carbon and nitrogen can migrate in structural materials/sodium systems as a result of chemical activity differences in isothermal or non-isothermal systems. Transfer of these elements also occurs in systems

where combinations of materials of different compositions are used [5]. Transfer of carbon in a non-isothermal sodium system can result in carburization/decarburization of ferritic steels, affecting both the microstructure and mechanical properties of the materials [5,6]. Chopra et al. [5] reported the conditions of temperature and carbon concentration in sodium for carburization/decarburization of Fe-9Cr-Mo steels, which are similar to those for austenitic stainless steels. It was shown that Fe-9Cr-Mo steels would decarburize in sodium with the carbon concentration $< \sim 2.5$ ppm at 650°C. Though the carbon concentration in sodium in our experiments was not measured, measurements of carbon concentration in sodium in similar sodium loops [5] indicated that the carbon concentration in sodium was < 1 ppm, and decarburization of optimized and commercial G92 was expected in our 650°C-sodium exposure tests.

The carbon transfer behaviour of Fe-9Cr-Mo steels is also sensitive to its composition and carbide structure. When the alloy is exposed to liquid sodium, the carbon activity between the alloy and the sodium environment must be equalized, and thermodynamically stable carbide phases are formed [5,6]. Both processes influence the kinetics of carburization and decarburization of the alloy in a liquid sodium environment, and the initial carbide structure and their subsequent changes have a major effect on the kinetics of carburization/decarburization in sodium [5,6]. Thermodynamic calculations showed that at 650°C the equilibrium phases are bcc-Fe, $M_{23}C_6$, Z-phase ((Cr,(V,Nb)N), and Laves phase in optimized and commercial G92. The MX phase formed during tempering in G92 is metastable and eventually transforms to the Z-phase. We observed a very low number density of MX precipitates and no Z-phase precipitates in the 650°C-sodium exposed specimen of Opt. G92-4, which may be related to the loss of carbon and nitrogen from the steel in sodium that facilitates the dissolution of the MX phase and inhibits the precipitation of the Z-phase. Thermo-mechanical treatments of optimized G92 can maximize nucleation sites for MX precipitates [1]. The similar corrosion behaviour and the effect of sodium exposures on tensile strength observed in two different heats of optimized G92, i.e. non-TMT Opt. G92-4 and TMT Opt. G92-4T imply that the initial thermo-mechanical treatment of optimized G92 has no significant effect on the evolution of MX in the sodium environment.

Coarsening and dissolution of $M_{23}C_6$ carbides observed in Opt. G92-4 exposed to sodium at 650°C may also be understood in terms of decarburization of optimized G92. Natesan et al. [4] reported that low-Cr ferritic steel would decarburize to a certain carbon level at the temperature corresponding to stable carbides, and subsequent decarburization would be controlled by the dissolution rate of the carbide phase in the ferrite matrix. Thermodynamic calculations have shown that reducing the carbon content in G92 will reduce the volume fraction of $M_{23}C_6$ carbides. The apparent more severe coarsening behaviour of $M_{23}C_6$ carbides in the sodium-exposed specimen than in the thermally-aged specimen of Opt. G92-4 is likely due to dissolution of smaller sizes of $M_{23}C_6$ particles in the sodium environment. The coarsening kinetics of $M_{23}C_6$ particles is mainly dependent on the temperature, time, initial particle size, and the interfacial energy of the carbide [8]. It is suggested that the dissolution of $M_{23}C_6$ carbides plays an important role in the overall carbon transfer process. Dissolution and coarsening of $M_{23}C_6$ particles can promote the recovery of martensite structure, resulting in reduced dislocation density and subgrain coarsening [7]. This is consistent with our observations and measurements of subgrains and dislocations in Opt. G92 after thermal and sodium exposures at 650°C (Fig. 4).

Formation of intermetallic Laves phase was observed in both the sodium-exposed and thermally-aged specimens at 650°C. According to the thermodynamic analysis, the

decarburization of G92 promotes the formation of Laves phase. A slightly higher area density of Laves phase was measured in the sodium-exposed Opt. G92-4 specimen than in the thermally-aged specimen.

Our experimental data show that the tensile strength of optimized and commercial G92 was significantly reduced by sodium exposures at 650°C, but not at 550-600°C. During the 650°C-sodium exposures, dislocation density decreased, subgrains coarsened, $M_{23}C_6$ and MX particles dissolved, and a new phase, intermetallic Laves phase formed. The interactive processes of these microstructural constituents contribute to the reduction of the tensile strength of G92. The dissolution and coarsening of $M_{23}C_6$ and MX particles during sodium exposure can weaken both sub-boundary strengthening and precipitation strengthening in G92. Precipitation of the Laves phase effectively removes W and Mo solute atoms from the ferrite matrix, diminishing the solid solution hardening in G92.

Fe-9Cr-Mo steels can either carburize or decarburize depending on the carbon activity in sodium and temperature [5,6]. When they are exposed to sodium at lower temperatures, e.g. 550-600°C, carburization tends to occur. Our tensile data have shown that sodium exposures at 550-600°C have minimal effects on the tensile properties of optimized and commercial G92. A study by Ito et al. [9] on the Japanese Mod. Fe-Cr-Mo steel found that no difference in tensile properties was observed between the sodium-exposed and thermally-aged materials containing 0.08-0.14 wt% C in spite of the presence of a thin carburized layer, consistent with our findings in the 550-600°C sodium exposure tests.

It should be noted that G92 ferritic-martensitic steels are predominantly used at temperatures <600°C for structural applications. Thermal and sodium exposures at 650°C are considered as accelerated tests for these steels. Long-term exposures of these alloys at lower temperatures of 550-600°C are needed to corroborate the understanding of the effect of sodium exposures gained from high-temperature accelerated tests.

5. Conclusion

Several heats of optimized Grade 92 with or without thermo-mechanical treatment were investigated in liquid sodium environments at 550-650°C to evaluate their long-term performance. Data of sodium-exposed specimens were compared with thermal aging data of the same heat of optimized Grade 92 to separate the effects of sodium exposures and thermal aging. Optimized Grade 92 showed an insignificant weight loss after exposures to sodium at 650°C, corresponding to a corrosion rate <1 $\mu\text{m}/\text{y}$. Sodium exposures at 550°C for up to ~11,000 h and 600°C for up to 16,000 h showed nearly no additional effect of sodium exposures on tensile properties relative to thermal aging of optimized and commercial G92; sodium exposures at 650°C in contrast, significantly reduced the tensile strength of optimized G92 and commercial G92 even after ~4,000 h, but not the total elongation. Microstructural characterization of optimized G92 after sodium and thermal exposures at 650°C showed pronounced subgrain coarsening, reduction of dislocation density, dissolution and coarsening of $M_{23}C_6$ and MX particles, and precipitation of Laves phase, which can reduce subgrain boundary hardening, MX precipitation hardening, and solid solution strengthening. The significant microstructural and tensile property changes observed at 650°C and minimal effects at lower temperatures may be understood by the decarburization/carburization behaviour of the alloy, and the dissolution of carbides and carbonitrides plays an important role in the carbon transfer process.

Acknowledgements

This research was sponsored by the U.S. Department of Energy, Office of Nuclear Energy, for the Advanced Reactor Technologies (ART) Program under Contract DE-AC02-06CH11357. We gratefully acknowledge the support provided by Carl Sink of DOE-NE, Advanced Reactor Technologies Program Manager; William Corwin of DOE-NE, Advanced Reactor Technologies, Materials Technology Lead; Robert Hill of Argonne National Laboratory, ART National Technical Director; and Sam Sham of Argonne National Laboratory, ART Materials Development Technical Area Lead. Use of the Center for Nanoscale Materials, an Office of Science user facility, was supported by the U. S. Department of Energy, Office of Science, Office of Basic Energy Sciences, under Contract No. DE-AC02-06CH11357.

Materials were provided by the Oak Ridge National Laboratory. David Rink is thanked for loop construction and operation, specimen preparation, post-exposure handling, and weight and dimension measurements. J. T. Listwan and Mark Quesinberry are thanked for conducting tensile tests.

The United States Government retains and the publisher, by accepting the article for publication, acknowledges that the United States Government retains a non-exclusive, paid-up, irrevocable, world-wide license to publish or reproduce the published form of this manuscript, or allow others to do so, for United States Government purposes.

References

- [1] L. TAN, et al., "Creep resistance and fracture toughness of recently-developed optimized G92 and its weldments for advanced fast reactors," IAEA-CN-245-50, 2017.
- [2] O. K. CHOPRA, K. NATESAN AND T. F. KASSNER, in: Proc. Intern. Conf. on Liquid Metal Technology in Energy Production, CONF-760503-P2 (1976), p. 730.
- [3] G. MENKEN, E. D. GROSSER AND E. TE HESSEN, in: Proc. Intern. Conf. on Ferritic Steels for Fast Reactor Steam Generators (BNES, London, 1978), p. 264.
- [4] K. NATESAN, O.K. CHOPRA, AND T. F. KASSNER, "Compatibility of Fe-2 ¼ wt% Cr- 1 wt% Mo steel in a sodium environment," Nucl. Tech. 28 (1976) p. 441.
- [5] O. K. CHOPRA, K. NATESAN, AND T. F. KASSNER, "Carbon and nitrogen transfer in Fe-9Cr-Mo ferritic steels exposed to a sodium environment," J. Nucl. Mater. 96 (1981) 269.
- [6] A. SALTELLI, O. K. CHORPA, AND K. NATESAN, "An assessment of carburization-decarburization behaviour of Fe-9Cr-Mo steels in a sodium environment," J. Nucl. Mater. 110 (1982) 1.
- [7] F. ABE, "Progress in creep-resistant steels for high efficiency coal-fired power plants," J. Press. Ves. Tech. 138 (2016) p. 040804-1.
- [8] J. HALD AND L. KORCAKOVA, "Precipitate stability in creep resistant ferritic steels – experimental investigations and modelling," ISIJ Inter. 43 (2003) p. 420.
- [9] T. ITO, S. KATO, M. AOKI, E. YOSHIDA, T. KOBAYASHI, and Y. WADA, "Evaluation of Carburization and Decarburization Behavior of Fe-9Cr-Mo Ferritic Steels in Sodium Environments," J. Nucl. Sc. And Technol. 29 (4), 367 (1992).